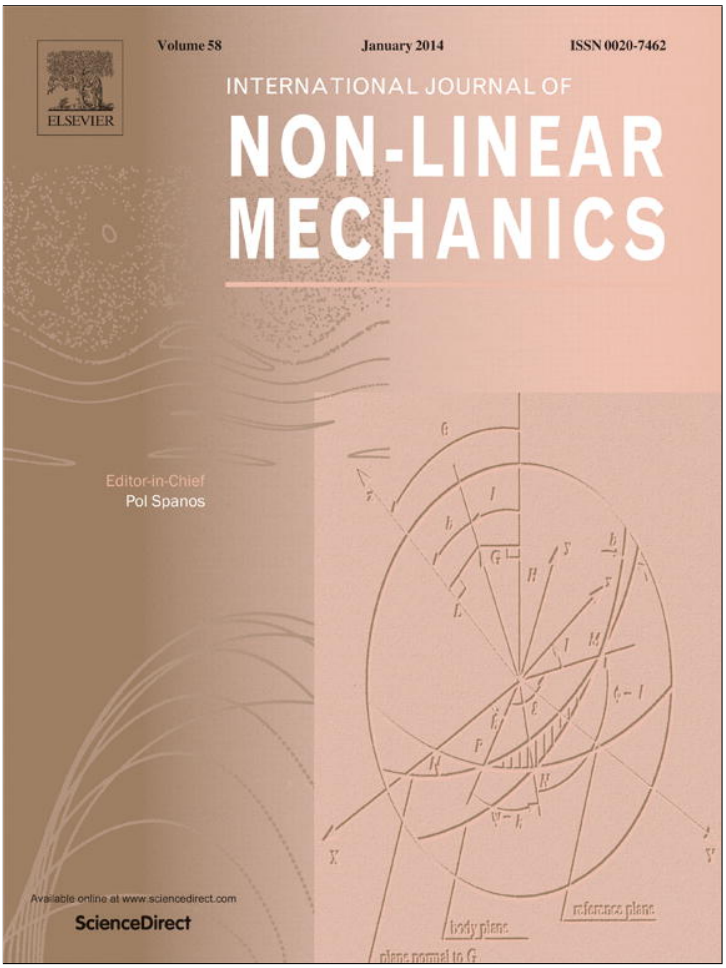

International Journal of Non-Linear Mechanics 58 (2014) 111–119

Contents lists available at ScienceDirect

International Journal of Non-Linear Mechanics

journal homepage: www.elsevier.com/locate/nlm

Modeling the interaction between contact mechanisms in normal and tangential directions

M. Bazrafshan [a], H. Ahmadian [a], H. Jalali [b,*]

[a] Centre of Excellence in Experimental Solid Mechanics and Dynamics, School of Mechanical Engineering, Iran University of Science and Technology, Tehran, Iran
[b] Department of Mechanical Engineering, Arak University of Technology, Arak 38135-1177, Iran

ARTICLE INFO

Article history:
Received 16 January 2013
Received in revised form
9 September 2013
Accepted 9 September 2013
Available online 18 September 2013

Keywords:
Friction reduction
Slip
Micro-vibro-impact
Contact tangential stiffness

ABSTRACT

Contact interface dynamics depends on contact surfaces characteristics and the interaction of these surfaces in normal and tangential directions. In fact the interaction in normal direction affects the behavior in tangential direction through changing the size of the contact area. The level of vibration in normal direction is inversely proportional to the contact stiffness in tangential direction and the friction force. In this paper the effects of micro-vibro-impact developing at the boundary of a non-linear beam on the parameters of micro-slip mechanism are studied. Also the variation of the contact stiffness in tangential direction is modeled as a function of vibration amplitude level.

1. Introduction

Non-linear dynamic simulation of mechanical structures has become a prominent point of interest during the past decades. The frictional contact interface is of the most remarkable source of non-linearity in structures. The development of a precise numerical method to simulate the non-linear mechanisms at contact interfaces and identification of their parameters are main concerns in structural response analysis. The contact interface dynamics depend on several factors [1] such as the sliding speed [2–4], surface roughness [5–12], temperature [1,14], normal force [12,15–20] and the dynamic interaction of the contacting bodies [21–27]. Precise modeling is possible when the above-mentioned factors are considered.

Stribeck [2] observed that the coefficient of friction has different behaviors in low and high relative velocities. The coefficient of friction is inversely dependent on the relative velocities. Heslot et al. [3] proposed a heuristic model of low velocity friction. In their model, creep process controls the low speed dynamics but at higher velocities, a crossover to inertial dynamics is observed. Liu et al. [4] presented a model treating both the elastohydrodynamic and the contact friction in lubricated rough circular contact. They showed that the friction parameters obtained by this model are in good agreement with the experimental Stribeck curves measured from a ball-on-disk test setup.

The friction parameters are influenced by surface texture and thus roughness parameters. Whereas, this influence is dependent on many factors, for instance, the presence of impurities or liquid films in the tribological contact, among others. One of the most important factors affecting the frictional parameters during sliding is surface texture. Plenty of attempts have been made to study this effect. Staph et al. [5] have studied the results of disk tests designed to examine the effect of surface texture and roughness on scuffing and related behavior. They observed that under different conditions, an increase in the composite surface roughness increases the friction coefficient at scuffing. The effects of surface roughness on lubricant film characteristics under conditions of combined normal and sliding motion have been studied in [6]. Mattaa et al. [7] used a new slider-on-strip tribometer to study the tribological behavior of traditional and new tool materials. They observed that the composition of the tool steel does not affect the friction between the tool and the work piece very much. However, the friction is notably influenced by the surface roughness and topography of the tool.

Temperature is another significant factor which can influence contact parameters. However, no model has been proposed to simulate the variation of these parameters with temperature, so far. Filipi et al. [13] investigated the variation of contact tangential stiffness under a wide range of contact normal loads, relative displacements, excitation frequencies and contact specimens. They observed that as the temperature increases the contact stiffness decreases. Schwingshackl et al. [14] designed a test rig to characterize

* Corresponding author. Tel.: +98 86 3670024.
E-mail address: jalali@iust.ac.ir (H. Jalali).

0020-7462/$ - see front matter © 2013 Elsevier Ltd. All rights reserved.
http://dx.doi.org/10.1016/j.ijnonlinmec.2013.09.002

Nomenclature

A	beam cross-sectional area
a	maximum response amplitude at driving point
b	beam width
d_p	excitation point distance from clamped end
E	beam elastic modulus
E_e	elastic modulus
E_p	plastic modulus
e_i	interface tangential stiffness in stick regime (Valanis model)
e_0	interface tangential stiffness in micro-slip regime (Valanis model)
$f(t)$	excitation force
h	beam thickness
I	area moment of inertia
J_p	mass moment of inertia of the pin
k_b	axial stiffness of the beam
KHC	stiffness constant in Hunt–Crossley model
L	beam length
mp	pin mass
ms	hanging block mass
N	number of samples used in optimization
$N(t)$	normal contact force
n	a constant number
n_{HC}	a constant number in Hunt–Crossley model
$qi(t)$	ith modal coordinate
r	pin radius
S	initial slope of moment–rotation curve
Sp	the slope of moment–rotation curve in high rotations
Sy	yield stress
$S(t)$	tangential contact force (friction force)
T	kinetic energy
u	axial displacement of the beam tip
V	potential energy
X	tangential displacement amplitude
Xy	tangential displacement amplitude in the beginning of macro-slip
$y(x,t)$	lateral deflection of the beam
Z	a physical parameter
ρ	mass density of the beam
σ	stress
ε	strain
$\eta(t)$	normal displacement of contact point
$\xi(t)$	tangential displacement of contact point
λHC	damping constant in Hunt–Crossley model
δ_0	static deflection of contact point due to preload
$-\delta Wnc$	work of non-conservative forces
φi	ith non-linear normal mode of the beam
p	vector of unknown parameters

friction contact interfaces. An intense reduction of friction coefficient from room temperature to 200 °C and a more or less constant trend thereafter was observed.

One of the other significant factors remarkably affecting the contact parameters is normal contact force. Through different methods of contact evaluation, it has been revealed by many researchers that regardless of the contact roughness, the contact tangential stiffness is non-linearly proportional to the normal contact load as a consequence of contact stiffness dependent on real contact area. Sextro [12] developed a contact model describing the variation of contact tangential stiffness vs. applied normal load for different amounts of contact roughness. Sherif and Kossa [15] investigated the effect of normal load on the normal and tangential stiffness between two elastic bodies. The measurement of ultrasonic waves' reflection from contact interfaces has been employed to characterize the contact parameters [16–18]. Jiang et al. [19] proposed a contact model based on fractal theory to investigate the contact topography and elastic–plastic deformation of asperities between rough surfaces of machined plane joints. Kartal et al. [20] proposed an experimental method to measure the contact tangential stiffness. They used the digital image correlation to measure the local displacement field. It was found that the tangential contact stiffness is approximately proportional to the nominal contact area and normal pressure.

Contact interfaces are usually subjected to dynamic loads; consequently the contact parameters are affected by the loading conditions. The aim of this paper is to investigate how dynamic normal loads influence the contact characteristics especially tangential contact stiffness. As an earlier attempt in this area, Godfrey [21] conducted some experiments to determine the effect of dynamic normal loads on tangential contact stiffness. In his experiments, a rider including three balls slides along a flat steel plate under some weight load. The plate was excited to vibrate at different frequencies by means of a speaker. Friction coefficient, acceleration and electrical resistance of the contact interface were measured. It was observed that whether the contact interface is lubricated or not, the apparent kinetic friction decreased rapidly after that the vibration acceleration exceeded the gravity acceleration. Using an empirical stiffness relation, Tolstoi et al. [22,22] modeled the contact interface between two surfaces as a non-linear spring. It was theoretically and experimentally shown that the friction reduction due to normal vibration could reach 30% for various steel surfaces. Tolstoi [22] experimentally showed that by exciting the sliding pair by a swept sine wave, the average friction decreases when the contact was driven at its normal contact frequency. Hess and Soom [24] studied the non-linear vibration at a Hertzian contact by using the multiple scales method. They found that as a result of Hertzian stiffness, the average normal contact deflection during vibration is smaller than the static one under the same average load. This shows that the normal vibration leads to a reduction of the average area in contact and consequently the friction force. Chowdhury and Helali [25,26] experimentally investigated the effect of external vertical vibration on the friction property of mild steel, glass fiber-reinforced plastic and cloth-reinforced ebonite. Their results showed that the friction coefficient decreases with the increase of the frequency and amplitude of vertical vibration for the above-mentioned materials. Kostek [27] studied the influence of an external normal harmonic force upon friction force reduction for a system consisting of two bodies in planar contact. He concluded that the main reason of reduction in friction force is dynamical effect, e.g. stick-slip regime.

In this paper the effect of vibration in normal direction of a contact interface on the contact parameters in tangential direction is studied. The stiffness in stick regime of the contact interface in tangential direction is formulated by employing the model proposed by Richard and Abbott [28]. This model is based on a formula to reproduce the elastic–plastic behavior of materials and has initially been used to simulate the static monotonic response of joints [29]. The remaining of this paper goes as follows: in Section 2, a brief explanation of non-linear mechanisms at contact interfaces is presented. Section 3 deals with the experimental case study and mathematical modeling. In Sections 4 and 5, parameter identification of the contact interface is considered and the variation of tangential contact stiffness is modeled. Finally the conclusions are drawn and references are presented.

2. The contact interface dynamics

The non-linear nature of the contact interfaces can be attributed to two mechanisms: micro-/macro-slip and vibro-impact (slap) mechanisms. Slip occurs when two adjacent surfaces in contact move tangentially relative to each other as the consequence of an external applied load. Depending on the level of applied load, contact interface may experience three different regimes: stick, micro-slip or macro-slip regimes. Under low level of vibration amplitudes the interface is in stick and its behavior is linear. By increasing gradually the level of vibration, small regions in the contact interface begin to slip which is called micro-slip. Eventually when all area in contact starts to slip, macro-slip occurs.

Among several models ever been proposed for taking into account the effect of slip mechanism in mathematical representation of the structures, Valanis model [30,31] has received more attention during the past decades. In this model a non-linear differential equation governs the tangential force in contact interface, i.e.

$$\dot{S}=\frac{e_0\dot{\xi}\left[1+\frac{\lambda}{e_0}\mathrm{sgn}(\dot{\xi})(e_t\xi-S)\right]}{1+\kappa\frac{\lambda}{e_0}\mathrm{sgn}(\dot{\xi})(e_t\xi-S)},\quad \lambda=\frac{e_0}{\alpha_0\left(1-\kappa\frac{e_t}{e_0}\right)} \tag{1}$$

where S is the contact tangential force, ξ and $\dot{\xi}$ are relative tangential displacement and velocity, respectively, e_0 and e_t are the contact shear stiffness in stick and macro-slip regimes, κ is a control parameter to define a smooth transition from stick regime to macro-slip due to micro-slip in the contact interface and α_0 sets the yield point in the contact interface hysteresis loop, i.e. the diagram of contact force vs. relative displacement.

As a result of differential structure of Valanis model, slip force in each moment depends on not only the states at that moment but also the previous states, which is a distinct characteristic of friction phenomenon. Also, the Valanis model uses relatively minimum number of parameters among the other friction models to describe the friction phenomenon. This is especially important when optimization algorithms have to be used for parameter identification. The parameters of the Valanis model have physical meaning and can be interpreted by using the hysteresis loop of friction force. These properties make the Valanis model suitable for representing the slip mechanism in structures.

Under high level of vibrations, vibro-impacts (or slaps) happen in contact interfaces. This phenomenon develops when nearby zones of the contact interface move toward each other reciprocally. When these zones completely separate from each other and come to contact repeatedly, macro-vibro-impact (macro-slap) takes place. Micro-vibro-impact (micro-slap) develops when the applied external force is not high enough to completely separate the adjacent surfaces from each other. In this condition microscopic impacts develop between contact surfaces and a small amount of energy is dissipated by this mechanism [32]. Fig. 1 shows the region of contact at which micro-impact happens. As these local impacts with variable area in contact occur repeatedly, micro-vibro-impact mechanism develops.

The most widely used model to represent the normal force during impact is Hunt–Crossley model [33] which is based on the Hertzian contact theory. Considering micro-impact as a part of a complete impact in which the contact surfaces do not separate from each other completely, one can employ this model to take into account the effect of vibratory normal force. The contact normal force by this model is expressed as

$$N(t)=K_{HC}(\delta+\delta_0)^{n_{HC}}(1+\lambda_{HC}\dot{\delta}) \tag{2}$$

where $N(t)$ is the contact normal force, δ and $\dot{\delta}$ are respectively the relative normal displacement and velocity in contact interface, K_{HC} and λ_{HC} are non-linear normal stiffness and damping coefficients. n_{HC} is a constant and δ_0 is the static deflection due to the constant normal force P_0 (see Fig. 1).

In above the dynamics of the contact interface in normal and tangential directions were investigated considering that the micro-slip mechanism in tangential direction does not affect the micro-vibro-impact mechanism in normal direction or vice-versa. In reality, however, it is not the case because after happening one of the above-mentioned mechanisms, the surface texture changes which results in the change of the parameters of the other mechanism. This is the subject which is dealt with in the remaining of this paper. In the next section a structure subjected to a contact interface is experimentally studied and its corresponding mathematical model is developed.

3. Experimental case study and mathematical modeling

In this section, the dynamic response of a cantilever beam being subjected to a frictional contact interface in its free end is employed to investigate the interaction between the contact mechanisms in normal and tangential directions. Fig. 2 shows a uniform slender beam which is clamped in its left boundary and is subjected to a frictional support in the right boundary.

A constant static force applied by means of a hanging mass block (not included in Fig. 2, see Fig. 4) is applied to the contact interface. The static force prevents the contact point from a complete lateral separation. Due to the weight load of this block, the contact point is subjected to an unknown static deflection named δ_0. This static deflection was added in the previous section to the original version of Hunt–Crossley model.

The structure is excited using a B&K4200 mini shaker attached through a stinger to the structure. A B&K8200 force transducer is placed between the stinger and the structure to measure the excitation force. The structural response is measured using three accelerometers installed on the beam at locations 530, 290 and 110 (measured from the beam clamped end). Two sets of experiments are performed on the beam: (1) low level random excitation is used to measure the linear FRFs and (2) single harmonic excitation forces at different response amplitude levels are employed to construct the non-linear FRFs and hence characterize the contact interface. The experimental results are presented in Fig. 3.

The above experimental results are used in constructing a precise mathematical model for the structure. The linear FRF is used to obtain a reference linear model and the non-linear FRFs are employed to construct the non-linear normal modes and to identify the parameters of the contact mechanisms. These are done through the remaining of this section and the next section.

Fig. 4 shows a mathematical representation of the structure depicted in Fig. 2. In Fig. 4 the lateral deflection of the beam and the axial displacement of the pin center are denoted by $y(x,t)$ and $u(t)$, respectively. Different parameters of the beam are tabulated in Table 1. Due to the lateral deformation of the beam and especially the pin rotation, the contact point is exposed to both tangential and normal displacements. One can obtain the following equations governing the lateral deflection of the beam using the extended Hamilton's principle (see the Appendix A for details):

$$\begin{aligned}&\rho A\ddot{y}(x,t)+EIy''''(x,t)+f(t)\delta(x-d_p)\\&\quad+[S(t)+(m_s+m_p)(\ddot{u}(t)+r\ddot{y}'(L,t)-\Im(t))\\&\quad-m_pr\ddot{y}'(L,t)]y''(x,t)=0\end{aligned} \tag{3}$$

$$\Im(t)=\frac{1}{2}\frac{\partial^2}{\partial t^2}\int_0^L y''(x,t)^2\,dx \tag{4}$$

$$(m_s+m_p)(\ddot{u}(t)+r\ddot{y}'(L,t)-\Im(t))-m_pr\ddot{y}'(L,t)+k_bu(t)+S(t)=0. \tag{5}$$

where $(\dot{\square})=\partial\square/\partial t$ and $(\square')=\partial\square/\partial x$. The tangential and normal loads at the contact interface are denoted by $S(t)$ and $N(t)$, respectively.

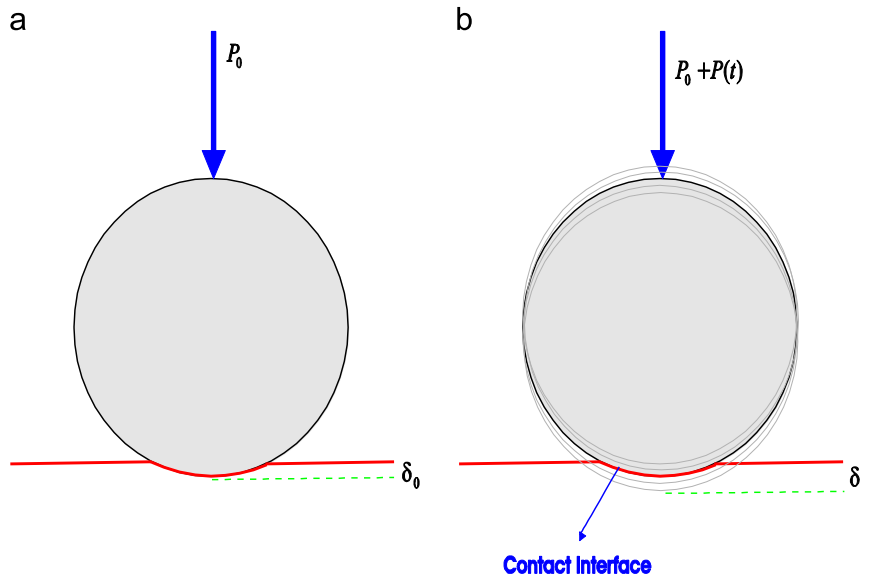

Fig. 1. The micro-vibro-impact mechanism due to the variable area in contact; (a): static loading and (b): dynamic loading.

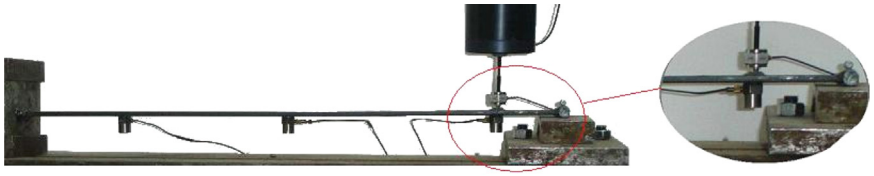

Fig. 2. The experimental test rig.

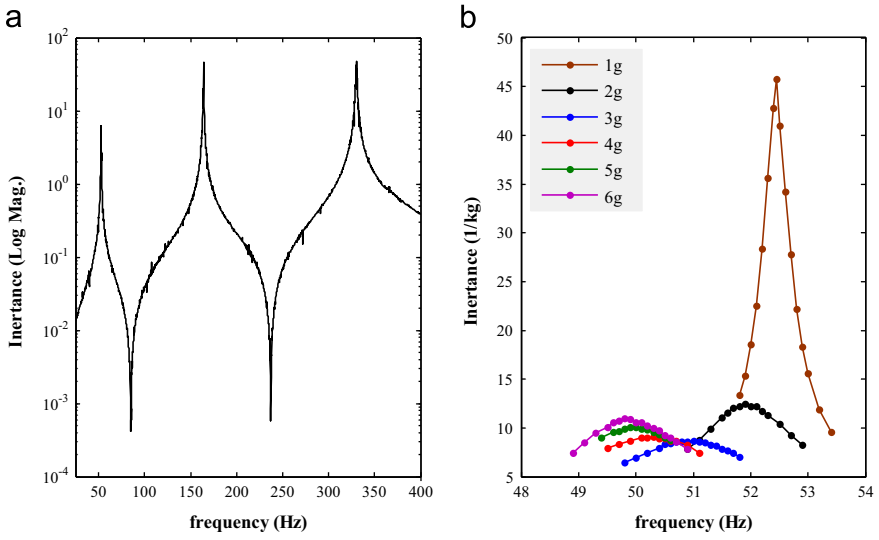

Fig. 3. Linear (a) and non-linear (b) FRFs at different response amplitude levels ($g = 9.81\ m/s^2$).

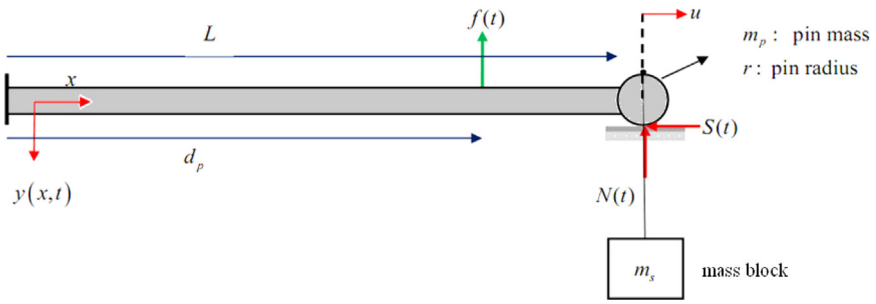

Fig. 4. Mathematical representation of the structure.

Table 1
The parameters of the beam structure.

Parameter	Value
L	600 mm
b	40 mm
h	5 mm
EI	86.25 kg m^4
ρ	7850 kg m^{-3}
m_s	10 kg
r	6 mm
m_p	35 g
J_p	630 g mm^2
d_p	530 mm

Eqs. (3) and (5) are subjected to the following boundary conditions:

$$y(0,t)=0, \quad y'(0,t)=0, \tag{6,7}$$

$$EIy'''(L,t)-(m_s+m_p)(\ddot{y}(L,t)+r\ddot{y}'(L,t))-N(t) +y'(L,t)[S(t)+(m_s+m_p)(\ddot{u}(t)+r\ddot{y}'(L,t)-\Im(t))-m_p r\ddot{y}'(L,t)]=0, \tag{8}$$

$$EIy''(L,t)+r(N(t)-S(t))+J_p\ddot{y}'(L,t) +(m_s+m_p)(\ddot{y}(L,t)+r\ddot{y}'(L,t)) +rm_s(\ddot{u}(t)+r\ddot{y}'(L,t)-\Im(t))=0 \tag{9}$$

where the tangential and normal deflection of the contact point are $\xi(t)$ and $\eta(t)$, respectively, and are defined as

$$\xi(t)=-\frac{1}{2}\int_0^L y'(x,t)^2\,dx+ry'(L,t)+u(t) \tag{10}$$

$$\eta(t)=y(L,t)+ry'(L,t) \tag{11}$$

In Eq. (10), the first term on the right hand side is the shortening effect of the beam due to its lateral bending motion. The second term is the relative motion of the beam tip, and the last one indicates the axial displacement of the pin center.

The external excitation force $f(t)$ is considered to be single harmonic and the excitation frequency is chosen near the first resonant point. Therefore, the non-linear response of the beam can be spanned using its first n non-linear normal modes $\{\omega_i(a),\varphi_i(x,a)\}$ as [34]

$$\begin{Bmatrix} y(x,t) \\ u(t) \end{Bmatrix}=\sum_{i=1}^{n}\begin{Bmatrix} \varphi_i(x,a) \\ u_i(a) \end{Bmatrix}q_i(t) \tag{12}$$

where $q_i(t)$ is the ith modal coordinate. The non-linear normal modes are equal to the normal modes of the corresponding linearized structure at the same response amplitude level. They are functions of the maximum response amplitude of the driving point, i.e. a

$$a=\max(y(d_p,t)) \tag{13}$$

One of the most common approaches for reducing the order of continuous or discrete models is the Galerkin method. The mode shapes of the reference linear system or the non-linear normal modes can be used as trial functions in Galerkin method. Details about non-linear normal modes calculation and reference linear system construction can be found in [34]. In order to implement the Galerkin method, the expansion series in Eq. (12) is substituted into non-linear governing Eqs. (3) and (5) and their projection on each individual non-linear normal modes is set to zero. This leads to n discrete ordinary differential equations as

$$\int_0^L \varphi_i\{\rho A\ddot{y}(x,t)+EIy''''(x,t)+f(t)\delta(x-d_p) +[S(t)+(m_s+m_p)(\ddot{u}(t)+r\ddot{y}'(L,t)-\Im(t))-m_p r\ddot{y}'(L,t)]y''(x,t)\} +u_i\{m_s(\ddot{u}(t)+r\ddot{y}'(L,t)-\Im(t))+k_b u(t)+S(t)\}=0, \quad i=1,2,\ldots,n. \tag{14}$$

Using integration by part twice in the first term of Eq. (14), the effects of boundary conditions, specially $N(t)$, appear in the obtained discrete model. Having measured the excitation force $f(t)$ and choosing a set of parameters for Valanis and Hunt–Crossley models, the obtained ordinary differential equations (i.e. Eq. (14)) can be solved in time domain and $q_i(t)$ can be determined. Back substituting $q_i(t)$ into Eq. (12), the beam deflection $y(x,t)$ is obtained. The parameters of the contact mechanisms are identified by comparing $y(x,t)$ with the experimentally measured beam response. The identification procedure is explained in next section.

4. Identification process and results

In this section the parameters of the Valanis and Hunt–Crossley models are identified by using the experimental results presented in the previous section. The identification is done by minimizing the differences between experimental and analytical/numerical results. The most commonly used method is to minimize the sum of square of the differences at all sample points [35,36]. In this study, the normalized root mean square error percentage of the predicted driving point acceleration time history $\hat{a}(p,t)$ with respect to its experimentally measured counterpart, i.e. $a(p,t)$, is used as the objective function. The objective function can be then expressed as

$$OF(p)=\frac{\sqrt{\sum_{i=1}^{N}\left(\frac{a(p,t_i)-\hat{a}(p,t_i)}{a(p,t_i)}\right)^2}}{N}\times 100 \tag{15}$$

where p and N are, respectively, the vector of unknown parameters and the number of samples used in identification.p consists of the parameters of the Valanis and Hunt–Crossley models, i.e. $p=[e_0,\ e_t,\ \lambda,\ \kappa,\ \delta_0,\ n_{HC},\ K_{HC},\ \lambda_{HC}]^T$. The objective function, in other words, shows the differences between experimental and analytical hysteresis loops of driving point excitation force vs. acceleration, since the analytical and experimental forces are exactly the same. In order to minimize the objective function and identify the contact interface parameters the Genetic Algorithm toolbox of MATLAB is used. It is worth mentioning that all parameters of P are scaled to be between 0 and 1 while being optimized.

Identification of the contact interface parameters is performed at different response amplitude levels. At early stages of the identification process, it is found that the sensitivity of the beam dynamic response to the parameters of the Valanis model is much higher than the parameters of the Hunt–Crossley model. This indicates that the nature of the contact mechanism in normal direction remains unchanged in the response interval used in the experiments. Therefore, the parameters of the Hunt–Crossley model are kept constant and are identified at the response amplitude level of 6g. At this level the contact interface experiences the most non-linear effects. The identified parameters for the Hunct–Crossley model are presented in Table 2.

Arz and Laville [37] experimentally showed that the parameters of the contact mechanism in normal direction are constant. They identified a unique set of parameters for different impact velocities. It should be noted that despite the fact that the parameters of the contact mechanism in normal direction are constant, the equivalent normal stiffness and damping coefficients of the contact interface are variable at different response levels since they are dependent upon the displacement in normal direction.

Having known the parameters of the Hunt–Crossley model from a response amplitude level of 6g, the parameters of the Valanis model are identified at different response amplitude levels (Table 3). Fig. 5 shows the convergence rate of the objective

Table 2
Hunt–Crossley model identified parameters.

$\delta_0 \times 10^8$ (m)	n_{HC}	$K_{HC} \times 10^{-14}$ (N m$^{-n_{HC}}$)	$\lambda_{HC} \times 10^{-3}$ (N s m$^{-(n_{HC}+1)}$)
14.21	1.86	5.41	7.23

Table 3
Valanis model parameters with $\kappa = 0.5$ ($g = 9.81$ m/s^2).

Response amplitude	$e_t \times 10^{-3}$ (N m^{-1})	$e_0 \times 10^{-6}$ (N m^{-1})	$\lambda \times 10^{-5}$ (m^{-1})
1g	8.4	6.37	1.62
2g	8.8	4.79	1.63
3g	8.3	3.97	1.66
4g	8.2	3.13	1.67
5g	8.2	2.71	1.70
6g	8.6	2.46	1.66

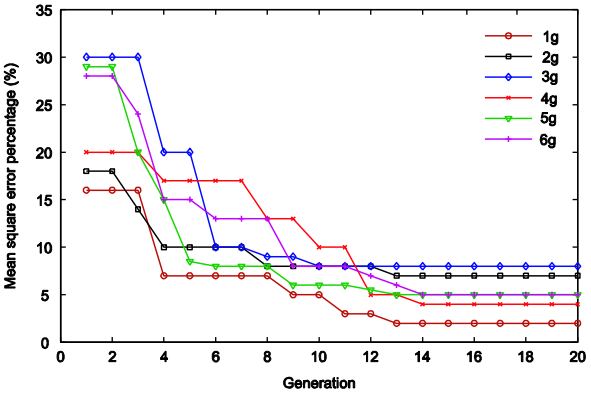

Fig. 5. Convergence rate of the objective function at different response amplitudes levels ($g = 9.81$ m/s^2).

function in identification process. Fig. 5 indicates that after 20 generations the minimization algorithm converges to an acceptable solution since the error is less than 8%.

It should be noted that by increasing the excitation level, the tangential displacement in contact interface is increased. This results in a decrease to the size of the stick regions and hence the contact tangential stiffness in stick regime decreases. This behavior is obviously observed in Table 3. As response amplitude level increases from 1g to 6g the contact tangential stiffness in stick, i.e. e_0, decreases gradually while the contact tangential stiffness in macro-slip, i.e. e_t, remains unchanged. Ahmadian et al. [34] showed that for the same contact interface, $e_t \approx 0$. This is used in the next section to develop a relation which considers the variation of the contact tangential stiffness in stick vs. the response amplitude level.

Using the identified parameters in Tables 2 and 3, Fig. 6 shows the hysteresis loops of excitation force vs. driving point acceleration at different levels of response amplitude. The results presented in Fig. 6 indicate that the differences between model predictions and experimental observations are negligible which shows the accuracy of the proposed method. Fig. 7 shows the slip force hysteresis loops at the contact point obtained from the analytical model with identified parameters. One should notice that as the response amplitude level increases, the initial slope of the hysteresis loops – representing the contact tangential stiffness in stick – decreases. It is also obvious that the final slope of hysteresis loops is negligible compared to their initial slopes.

The hysteresis loops of the normal force at the contact point are also depicted in Fig. 8. This figure indicates that by increasing the

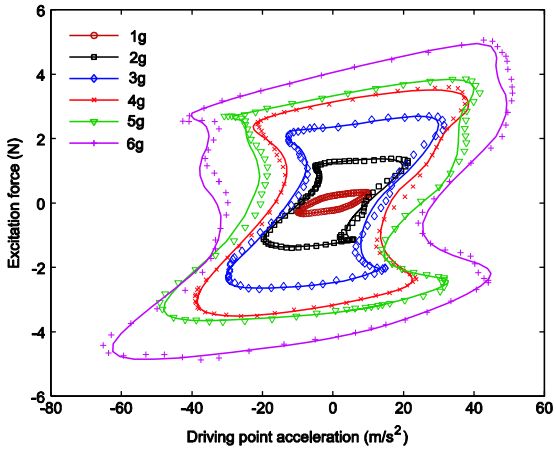

Fig. 6. Hysteresis loop of excitation force vs. driving point acceleration, model results (solid lines) and experiment results (dots) ($g = 9.81$ m/s^2).

excitation level the minimum value of the normal force approaches toward zero which shows that as the excitation level is increased the tendency of the contact interface in normal direction for separation is also increased. The next section deals with the variation of contact point tangential stiffness in stick regime, i.e. e_0, and a new relation will be proposed to relate this variation to the amplitude of contact point tangential displacement.

5. Contact tangential stiffness formulation

It was stated in the previous section that as a result of Hertzian normal contact stiffness, the average normal contact deflection during vibration is smaller than the static one under the same average load. Therefore the vibration in normal direction of the contact interface leads to the reduction of the average area in contact (see Fig. 1) and consequently the friction force. The main purpose of this section is to formulate the variation of contact point tangential stiffness in stick regime by using the Richard–Abbott model [28]. This model is based on the elastic–plastic behavior of materials. According to this model, the stress–strain ($\sigma - \varepsilon$) relation for elasto-plastic materials is expressed as

$$\sigma = \left((E_e - E_p)\left(1 + \left|\frac{(E_e - E_p)\varepsilon}{S_y}\right|^n\right)^{-(1/n)} + E_p\right)\varepsilon \tag{16}$$

where σ is the stress, ε is the strain, n is a constant number to control the transition from elastic to plastic state, S_y is the material yield stress, E_e and E_p are, respectively, elasticity and plasticity moduli. Fig. 9(a) shows the physical interpretation of these parameters. The initial and final slopes of stress–strain curve are elastic and plastic moduli of the material. Let us assume that $E_p/E_e \approx 0$ which shows the negligible amount of plastic modulus in comparison to the elastic modulus. Hence, one can easily obtain from Eq. (16) that

$$\sigma = E_e\left(1 + \left|\frac{E_e\varepsilon}{S_y}\right|^n\right)^{-(1/n)}, \quad \varepsilon = E_e\left(1 + \left|\frac{S}{S_y}\right|^n\right)^{-(1/n)}, \quad \varepsilon \equiv e_0(X)\varepsilon \tag{17}$$

where

$$e_0(X) = E_e\left(1 + \left|\frac{X}{X_y}\right|^n\right)^{-(1/n)} \tag{18}$$

Eq. (18) represents the general modulus of elasticity as a function of a physical parameter X. X_y is the specific amount of the physical parameter corresponding to the material yielding point. Eq. (18) includes three parameters E_e, X_y and n in which E_e is the initial value

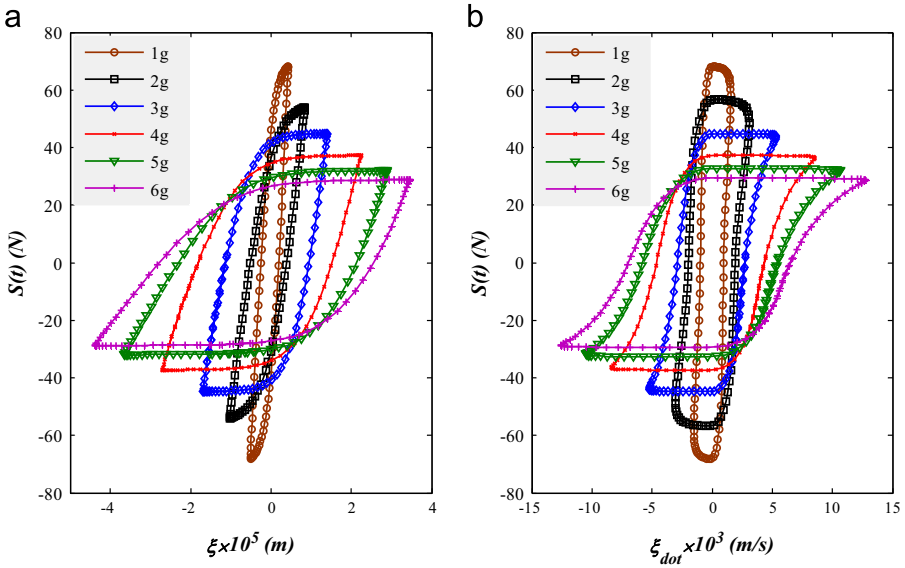

Fig. 7. Hysteresis loops of slip force at different levels of response amplitude ($g = 9.81$ m/s^2), (a) slip force vs. contact point tangential displacement and (b) slip force vs. contact point tangential velocity.

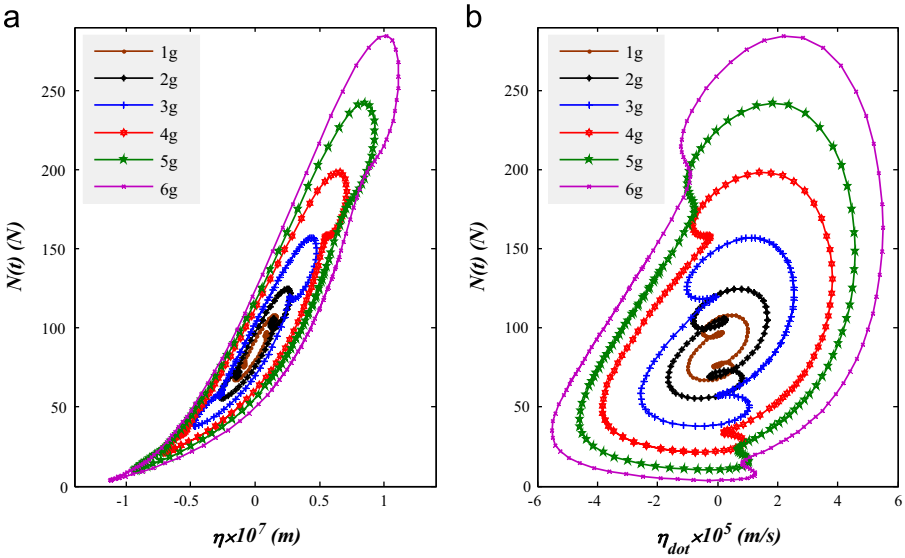

Fig. 8. Normal force hysteresis loops at different levels of response amplitude ($g = 9.81$ m/s^2), (a) normal force vs. contact point normal displacement and (b) normal force vs. contact point normal velocity.

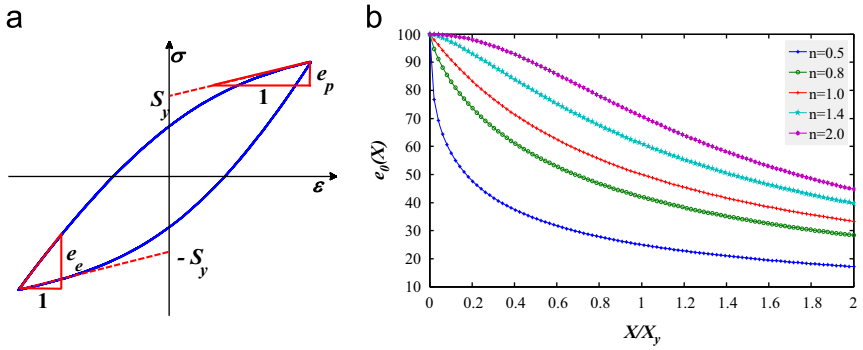

Fig. 9. (a) Stress–strain hysteresis loop and (b) typical curves of Eq. (18) for different values of n with $e_0 = 100$.

of the modulus of elasticity. Fig. 9(b) shows some typical curves of Eq. (18) for different values of n. An increase in X from zero to $2X_y$ leads to a decrease in e_0. The reduction rate of $e_0(X)$ depends on n.

As an analogy between stress–strain behavior of elasto-plastic materials and frictional contact interface behavior containing micro-slip to macro-slip regime, Eq. (16) can be used to predict

Table 4
The identified parameters corresponding to the proposed relation.

Parameter	Value
$E_e \times 10^{-6}$ (N m^{-1})	13.48
$X_y \times 10^{5}$ (m)	1.924
n	0.493

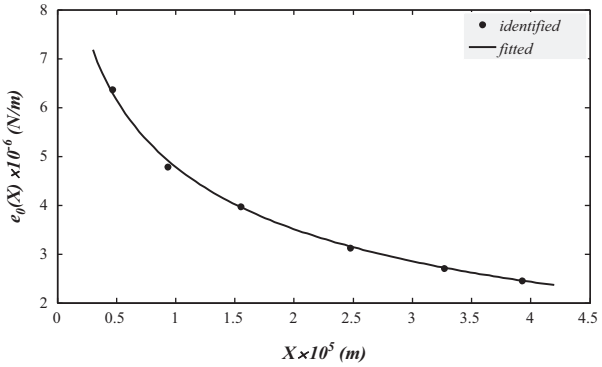

Fig. 10. Variation of contact point tangential stiffness in stick vs. tangential displacement amplitude.

the variation of contact point tangential stiffness. It should be noted that E_e, E_p, n and S_y of Richard–Abbott model are comparable with e_0, e_t, κ and α_0 of Valanis model. By using $E_p/E_e \approx 0$ according to the results presented in Table 3, Eq. (18) can be used to formulate the variation of contact point tangential stiffness. It is reasonable to consider X in Eq. (18) as the contact point tangential displacement amplitude. By curve fitting Eq. (18) in the results presented in Table 3 the unknown parameters are obtained as shown in Table 4. Fig. 10 depicts how contact tangential stiffness varies with tangential displacement amplitude. Good agreement between the identified values in the previous section (dots) and the predicted results by Eq. (18) (solid line) is observed in Fig. 10.

6. Conclusion

In this paper, the interaction between contact mechanisms in normal and tangential directions of a frictional contact interface was investigated. An experimental case study consisting of a clamped beam subjected to a frictional contact support at its free end was considered. The structural response of the beam to single frequency harmonic excitations and at different response amplitude levels was used to characterize the behavior of the contact interface in normal and tangential directions. Two models, i.e. Hunt–Crossley and Valanis models, were employed to represent the behavior of the contact interface. It was found that the parameters of the Hunt–Crossley model remain constant at different amplitude levels but the parameters of the Valanis model – especially the stiffness in stick regime – is response amplitude dependent. Finally, the variation of the stiffness in stick regime of the Valanis model was formulated.

Appendix A

The extended Hamilton's principle is employed to derive the governing equations of the system as shown in Fig. 4

$$\int_{t_1}^{t_2} (-\delta T + \delta V - \delta W_{nc})\, dt = 0 \tag{A.1}$$

The kinetic energy is defined as

$$T = \frac{1}{2}\left[\int_0^L \rho A \dot{y}(x,t)^2\, dx + (m_s+m_p)(\dot{y}_L + r\dot{y}'(L,t))^2 + J_p(\dot{y}'(L,t))^2\right] + \frac{1}{2}m_s\left(\dot{u} + r\dot{y}'(L,t) - \frac{1}{2\partial t}\int_0^L y'(x,t)^2\, dx\right)^2 + \frac{1}{2}m_p\left(\dot{u} - \frac{1}{2\partial t}\int_0^L y'(x,t)^2\, dx\right)^2. \tag{A.2}$$

The potential energy is as follows:

$$V = \frac{1}{2}\int_0^L EI(y''(x,t))^2\, dx + \frac{1}{2}k_b u^2. \tag{A.3}$$

Based on the fact that $S(t)$ and $N(t)$ are generally non-conservative forces, the virtual work of non-conservative forces is expressed as

$$-\delta W_{nc.} = S(t)\left[-\int_0^L y'(x,t)\delta y'(x,t)\, dx + \delta u - r\delta y'(L,t)\right] + N(t)(\delta y(L,t) + r\delta y'(L,t)) + \int_0^L f(t)\delta(x-d_p)\delta y(L,t)\, dx. \tag{A.4}$$

Substituting (Eqs. (A.2)–(A.4)) into Eq. (A.1) and after some algebraic manipulations and integration by part, one can obtain

$$\int_{t_1}^{t_2}\left\{\int_0^L (\rho A\ddot{y}(x,t) + EIy''''(x,t) + f(t)\delta(x-d_p) + [S(t) + (m_s+m_p)(\ddot{u} + r\ddot{y}'(L,t) - \Im(t)) - m_p r\ddot{y}'(L,t)]y''(L,t))\delta y(x,t) + ((m_s+m_p)(\ddot{u} + r\ddot{y}'(L,t) - \Im(t)) - m_p r\ddot{y}'(L,t) + k_b u + S(t))\delta u(t) - (EIy'''(L,t) - (m_s+m_p)(\ddot{y}(L,t) + r\ddot{y}'(L,t)) - N(t) + y'(L,t)[S(t) + (m_s+m_p)(\ddot{u} + r\ddot{y}'(L,t) - \Im(t)) - m_p r\ddot{y}'(L,t)])\delta y(L,t) + (EIy''(L,t) + r(N(t) - S(t)) + J_p\ddot{y}'(L,t) + (m_s+m_p)(\ddot{y}(L,t) + r\ddot{y}'(L,t)) + rm_s(\ddot{u} + r\ddot{y}'(L,t) - \Im(t)))\delta y'(L,t)\right\} dt = 0 \tag{A.5}$$

Separating the terms related to variations of independent coordinates, Eqs. (3)–(5) are obtained.

References

[1] V.L. Popov, Contact mechanics and friction, physical principles and applications, Springer-Verlag, Berlin, Heidelberg, 2010.
[2] R. Stribeck, Die wesentlichen eigenschaften der gleit-und rollenlager, Zeitschrift des Vereins Deutscher Ingenieure (1902).
[3] F. Heslot, T. Baumberger, B. Perrin, B. Caroli, C. Caroli, Creep, stick-slip and dry friction dynamics, experiments and a heuristic model, Physical Review E 49 (1994) 4973–4990.
[4] Q. Liu, W.T. Napel, J.H. Tripp, P.M. Lugt, R. Meeuwenoord, Friction in highly loaded mixed lubricated point contacts, Tribology Transactions 52 (2009) 360–369.
[5] H.E. Staph, P.M. Ku, H.J. Carper, Effect of surface roughness and surface texture on scuffing, Mechanisms and Machine Theory 8 (1973) 197–208.
[6] J. Lundberg, Influence of surface roughness on normal sliding lubrication, International Journal of Tribology 28 (1995) 317–322.
[7] A Maatta, P. Vuristo, T. Mantyla, Friction and adhesion of stainless steel strip against tool steels in unlubricated sliding with high contact load, International Journal of Tribology 34 (2001) 779–786.
[8] P.L. Menezes, S.V. Kishore, Kailas, Influence of surface texture on coefficient of friction and transfer layer deformation during sliding of pure magnesium pin on 080 M40 (EN8) steel plate, Wear 261 (2006) 578–591.
[9] W. Wieleba, The statistical correlation of the coefficient of friction and wear rate of PTFE composites with steel counterface roughness and hardness, Wear 252 (2002) 719–729.
[10] R. Singh, S.N. Melkote, F. Hashimoto, Frictional response of precision finished surface in pure sliding, Wear 258 (2005) 1500–1509.
[11] P.L. Menezes, Kishore, S.V. Kailas, , Influence of roughness parameters on coefficient of friction under lubricated conditions, Sadhana 33 (2008) 181–190.
[12] W. Sextro, Dynamical Contact Problems with Frictions, Models, Methods, Experiments and Applications, Springer-Verlag, New York, Berlin, Heidelberg, 2002.
[13] S. Filippi, E.B. Rodrigues, M.M. Gola, Experimental characterization contact hysteresis at high temperatures, in: Proceedings of the GT2006, Barcelona, Spain, 2006.
[14] C.W. Schwingshackl, E.P. Petrov, D.J. Ewins, Measured and estimated friction interface parameters in a nonlinear dynamic analysis, Mechanical Systems and Signal Processing, 28 (2012) 574–584.

[15] H.A. Sherif, S.S. Kossa, Relationship between normal and tangential contact stiffness of nominally flat surfaces, Wear 151 (1991) 49–62.
[16] B.W. Drinkwater, R.S. Dwyer-Joyce, P. Cawley, A study of the interaction between ultrasound and a partially contacting solid–solid interface, Mathematical, Physical & Engineering Sciences 452 (1996) 2613–2628.
[17] S. Biwa, S. Hiraiwa, E. Matsumoto, Stiffness evaluation of contacting surfaces by bulk and interface waves, Ultrasonic 47 (2007) 123–129.
[18] C. Putignano, M. Ciavarella, J.R. Barber, Frictional energy dissipation in contact of nominally flat rough surfaces under harmonically varying loads, Journal of Mechanics and Physics of Solids 59 (2011) 2442–2454.
[19] S. Jiang, Y. Zheng, H. Zhu, A contact stiffness model of machined plane joint based on fractal theory, Journal of Tribology, Transaction of ASME 132 (2010) 1–7.
[20] M.E. Kartal, D.M. Mulvihill, D. Nowell, D.A. Hills, Measurement of pressure and area dependent tangential contact stiffness between rough surfaces using digital image correlation, Tribology International 44 (2011) 1188–1198.
[21] D. Godfrey, Vibration reduces metal to metal contact and causes an apparent reduction in friction, ALSE Transaction 10 (1967) 183–192.
[22] D.M. Tolstoi, Significance of the normal degree of freedom and natural normal vibrations in contact friction, Wear 10 (1967) 199–213.
[23] D.M. Tolstoi, G.A. Borisova, S.R. Grigorova, Friction reduction by perpendicular oscillation, Soviet Physical-Doklady 17 (1973) 907–909.
[24] D.P. Hess, A. Soom, Normal vibrations and friction under harmonic loads. Part I: Hertzian contacts, Journal of Tribology, Transaction of ASME 113 (1991) 80–86.
[25] M.A. Chowdhury, M.M. Helali, The effect of amplitude of vibration on the coefficient of friction for different materials, Tribology International 41 (2008) 307–314.
[26] M.A. Chowdhury, M.M. Helali, The frictional behavior of materials under vertical vibration, Industrial Lubrication and Tribology 61 (2009) 154–160.
[27] R. Kostek, Influence of an external normal harmonic force on reduction of friction force, Journal of POLISH CIMAC 4 (2009) 67–73.
[28] R.M. Richard, B.J. Abbott, Versatile elastic-plastic stress-strain formula, Journal of Engineering Mechanics Division, ASCE 101 (1975) 511–515.
[29] R. Simoes, L. Simoes da Silva, Cyclic behavior of end-plate beam-to-column composite joints, Steel and Composite Structures 1 (2001) 355–376.
[30] K.C. Valanis, A theory of visco-plasticity without a yield surface, Archives of Mechanics 23 (1971) 171–191.
[31] L. Gaul, J. Lenz, Nonlinear dynamics of structures assembled by bolted joints, Acta Mechanica 125 (1997) 169–181.
[32] H. Jalali, H. Ahmadian, F. Pourahmadian, Identification of micro-vibro-impacts at boundary condition of a nonlinear beam, Journal of Mechanical Systems and Signal Processing 25 (2011) 1073–1085.
[33] K.H. Hunt, F.R.E. Crossley, Coefficient of restitution interpreted as damping in vibro-impact, Journal of Applied Mechanics 42 (1975) 440–445.
[34] H. Ahmadian, H. Jalali, F. Pourahmadian, Nonlinear model identification of a frictional contact support, Journal of Mechanical Systems and Signal Processing 24 (2010) 2844–2854.
[35] A.E. Charalampakis, V.K. Koumousis, Identification of Bouc-Wen hysteresis systems by a hybrid evolutionary slgorithm, Journal of Sound and Vibration 314 (2008) 571–585.
[36] R. Ying, The analysis and identification of friction joint parameters in the dynamic response of structures, Ph.D. Thesis, Imperial College of Science, Technology and Medicine, University of London, London, 1992.
[37] J.P. Arz, F. Laville, Experimental characterization of small thickness elastomeric layers submitted to impact loading, Journal of Sound and Vibration 326 (2009) 302–313.